Atomistic Simulations of Crystallization and Aging of GeTe Nanowires

S. Gabardi,[†] E. Baldi,[†,§] E. Bosoni,[†,‖] D. Campi,[†,⊥] S. Caravati,[†] G. C. Sosso,[‡] J. Behler,[¶] and M. Bernasconi[*,†]

[†]Dipartimento di Scienza dei Materiali, Università di Milano-Bicocca, Via R. Cozzi 55, I-20125 Milano, Italy

[‡]Thomas Young Centre, London Centre for Nanotechnology and Department of Physics and Astronomy, University College London, Gower Street WC1E 6BT London, U.K.

[¶]Universität Göttingen, Institut für Physikalische Chemie, Theoretische Chemie, Tammannstr. 6, 37077 Göttingen, Germany

[§]Current address: Laboratoire de science computationnelle et modèlisation (COSMO), École Polytechnique Fédéral Lausanne, CH-1015 Lausanne, Switzerland

[‖]Current address: School of Physics and CRANN, Trinity College Dublin, Dublin 2, Ireland

[⊥]Current address: Theory and Simulation of Materials (THEOS), École Polytechnique Fédéral Lausanne, CH-1015 Lausanne, Switzerland

E-mail: marco.bernasconi@unimib.it

Abstract

Nanowires made of chalcogenide alloys are of interest for application in phase change non-volatile memories. For this application insights into their thermal properties and in particular into the crystallization kinetics at the atomic level are crucial. To this aim, we have performed large scale atomistic simulations of ultrathin nanowires (9 nm in diameter) of the prototypical phase change compound GeTe. We made use

1

of an interatomic potential generated with a Neural Network fitting of a large ab-initio database to compute the thermal properties of the nanowires. By melting a portion of the nanowire, we investigated the velocity of recrystallization as a function of temperature. The simulations show that the melting temperature of the nanowire is about 100 K below the melting of the bulk which yields a reduction by about a factor two in the maximum crystallization speed. Further, the analysis of the structural properties of the amorphous phase of the nanowire suggests a possible origin of the reduction of the resistance drift observed experimentally in nanowires with respect to the bulk.

Introduction

Phase Change Memories (PCMs) are emerging as leading contenders for storage class memories that are sought to fill the performance gap between volatile dynamic random access memory (DRAM) and non-volatile Flash memories.[1] The active material in PCMs is a chalcogenide alloy, typically $Ge_2Sb_2Te_5$ (GST), with a low field resistance that changes by about three orders of magnitude across a reversible and fast crystalline-to-amorphous transformation.[2–6] Read out of the memory consists of a measurement of the resistance at low bias suitable to discriminate between the low resistive crystal and the high resistive amorphous phase. Joule heating at higher voltage induces the phase change, either the amorphization of the crystal (reset process) via crystal melting, or the recrystallization of the amorphous phase (set process).

Important issues for the development of storage class memories are the overall reduction of cell size and of power consumption for the set/reset processes. A very attractive option in this respect involves the change of the PCM geometry by using nanowires (NWs)[7,8] owing to their higher crystallinity and controllable sizes down to very low scale. Many studies have been devoted indeed to the synthesis and electrical characterization of GeSbTe,[7,9–13] GeSb,[14] Sb_2Te_3,,[15–17] and GeTe[13,15,18–24] NWs. Ultrathin InSbTe NWs with diameter below 15 nm have also been synthesized recently by metal organic chemical vapor deposition methods (MOCVD).[25] Moreover, core-shell NWs made of two materials with different melting/crystallization temperatures have been shown to provide a suitable realization of a multibit cell.[26,27] The reset currents decrease with the NWs size due to the reduction of cross-sectional area, heat and electric current confinement effects[8] and also because of a reduction of the melting temperatures with decreasing NW thickness.[21,28] A crystalline-to-amorphous transformation has also been achieved without melting in GST and GeTe NWs with significantly lower reset currents thanks to the formation, drift and jamming of dislocations produced by the electrical pulses.[29,30] Measurements of the recrystallization time under isothermal conditions revealed that recrystallization for thinner GST nanowires is

faster with a lower activation energy in comparison with thicker ones.[7] This feature has been ascribed to a higher heterogeneous crystal nucleation rate at the surfaces of the NWs with respect to the bulk which leads to an enhancement of the nucleation rate by increasing the surface-to-volume ratio.[9]

However, one might conceive a device geometry in which only a small portion at the center of the nanowire length undergoes the crystal-to-amorphous transformation due to self-heating (with no heater device). In the set operation, the temperature of this region would be rapidly brought above the glass temperature T_g as it is realized in conventional PCM. One would then realize a situation in which a small portion of supercooled liquid is in contact with a crystalline phase. Under these conditions, heterogeneous crystal nucleation at the nanowire surface would compete with crystal growth from the crystal/amorphous (crystal/liquid) interface.

Another advantage of the use of NWs is the reduction of structural relaxations in the amorphous phase with respect to the bulk.[31] In fact, while the crystal is stable, the metastable amorphous phase is subject to aging which leads to an increase in the electrical resistivity with time. This phenomenon called drift[32] is detrimental for the operation of PCM device and it has been shown to be substantially reduced in NWs with respect to the bulk.[33]

In this work we aim at providing an atomistic understanding of the different crystallization and aging behavior of NW with respect to the bulk under the conditions described above by means of molecular dynamics simulations.

We focus on the GeTe compound which shares a number of functional properties with the most studied GeSbTe ternary alloys. The simulations are performed with an efficient interatomic potential which allows handling systems containing several thousands of atoms. The potential has been generated by fitting a high-dimensional neural network (NN)[34,35] to the total energies of a large database of reference structures computed within Density Functional Theory (DFT).

After the brief outline of the computational methods in Sec. II, and of the choice of

4

the NWs geometry in Sec. IIIA, we report in Sec IIIB the results on the crystallization properties of GeTe NWs. The comparison of the structural properties of the amorphous phase of GeTe in the nanowire and in the bulk reported in Sec. IIIC suggests a possible origin for the reduced resistance drift measured experimentally in chalcogenide NWs. The analysis is based on the results of our previous study of this phenomenon in the bulk.[36]

Methods

We performed large scale molecular dynamics simulations by taking advantage of a machine-learning based interatomic potential generated by fitting a database of DFT energies by means of the Neural Network method introduced by Behler and Parrinello.[35] Our starting point was the NN potential obtained in Ref.[34] which is suitable to reproduce the bulk properties of GeTe. The database used in Ref.[34] consists of the total energies of about 30.000 configurations of 64-, 96-, and 216-atom supercells computed within DFT by employing the Perdew−Burke−Ernzerhof (PBE) exchange and correlation functional[37] and norm conserving pseudopotentials. As shown in Ref.[34] the NN potential displays an accuracy close to that of the underlying DFT-PBE framework whose reliability in describing structural and dynamical properties of GeTe and other phase change materials has been validated in several previous works.[38–41] The transferability of the NN potential has been validated in previous works for bulk liquid, amorphous, and crystalline GeTe.[34,42,43] By employing this potential we gained crucial information on the fragility of the supercooled liquid phase[44,45] and on the homogeneous[46] and heterogeneous[47] crystallization in the bulk.

The NN potentials provide a very accurate method to interpolate a given set of reference data from electronic structure calculations. However, they are not always reliable in describing structures very different from those used in the training set. For example, the NN potential constructed for bulk GeTe in Ref.[34] is very likely to fail when applied to surfaces or clusters. To deal with NWs, we have thus generated a new NN potential for GeTe by adding

in the training set 5000 new configurations of crystalline and amorphous GeTe in a slab geometry (128-atom supercell) and about 7000 new configurations of crystalline, amorphous and liquid GeTe in a NW geometry (120- and 256-atoms cells).

The 256-atom amorphous NW depicted in Fig. S1 in the Supplementary Information (SI) has been used to validate the potential. Pair correlation functions and angle distribution functions from DFT and NN simulations of the NW are reported in Figs. S2 and S3 in SI. The new potential also improves the description of bulk crystalline GeTe as shown in Table S1 in SI and performs similarly to the older one[34] for bulk amorphous and liquid phases (see Figs. S4-S5 in SI).

The NW geometry chosen for the simulations is described in Sec. IIIA. The simulations were performed with the NN code RuNNer[48] and by using the DL_POLY code as MD driver.[49] The time step was set to 2 fs and temperature was enforced by a stochastic thermostat.[50]

Results & Discussion

Modeling of GeTe Nanowires

At normal conditions GeTe crystallizes in a trigonal geometry (space group $R3m$, see Table S1 in SI).[51] This phase named α-GeTe, with two atoms per unit cell, can be viewed as a distorted rocksalt geometry with an elongation of the cube diagonal along the [111] direction and an off-center displacement of the inner Te atom along the [111] direction giving rise to a 3+3 coordination of Ge with three short and stronger bonds (2.84 Å) and three long and weaker (3.17 Å) bonds. In the conventional hexagonal unit cell of the trigonal phase, the structure can be also seen as an arrangement of GeTe bilayers along the c direction with shorter intrabilayer bonds and longer interbilayers bonds (see Fig. 1). The trigonal phase transforms into the cubic paraelectric phase (β-GeTe, space group Fm$\bar{3}$m) above the Curie temperature of 705 K.[52] In the cubic phase, the alternation of long and short bonds partially

survives in a disordered manner along all equivalent ¡111¿ directions as revealed by extended x-ray absorption fine structure (EXAFS) and x-ray total diffraction measurements.[53,54]
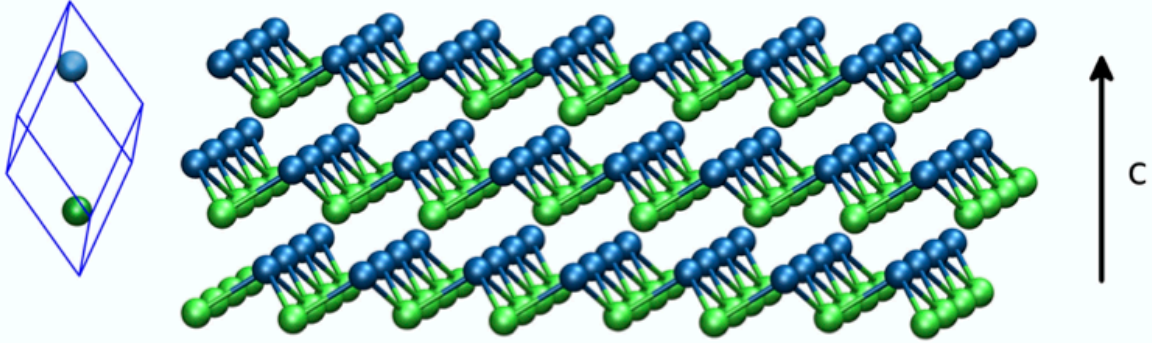

Figure 1: Geometry of the GeTe crystal seen as a stacking of bilayers along the c axis of the conventional hexagonal unit cell with the three short intrabilayers bonds and three long interbilayers bonds (see Table S1 in SI). Blue (dark) spheres denote Ge atoms and green (light) spheres denote Te atoms. The trigonal cell with two atoms is shiwn on the left.

GeTe nanowires have been grown by the vaporliquidsolid process with the [220] growth direction (in the hexagonal notation with the redundant index omitted) and diameters in the range 20-200 nm.[18–20] Single crystal α-GeTe nanowires with other growth directions have also been synthesized.[13,15,23,24] GeTe nanowires in the cubic phase have been grown along the [110] direction[21,22] which is equivalent to the [220] direction of the α phase. Therefore we decided to simulate an ultrathin α-GeTe nanowire grown along the [220] direction as in experiments.

To investigate the crystallization kinetics we had to perform several simulations at different temperatures, each about one ns long. Due to the high computational load, the simulation cell had to be limited to about 15000 atoms which implies a NW diameter below 10 nm. A single crystal NW of this size is expected to expose well defined crystalline surfaces.

We selected the surfaces to be exposed by simulating NWs with different shapes at high temperatures. We then selected the surfaces that do not undergo melting or strong disordering in runs 30 ps long at 800 K. The experimental melting temperature, T_m, is 998 K.[55] Among the five surface planes containing the [220] growth direction, indicated in Fig.

2a, the stable ones turn out to be the (001) and the (1$\bar{1}$2) surfaces. Moreover, the surfaces exposing Te atoms are more stable than those exposing Ge atoms, consistently with their lower DFT surface energies obtained in Ref.[56] This analysis suggested as a first guess for the NW geometry the hexagonal shape shown in Fig. 2b. We then annealed at 300 K and then optimized at 0 K the geometry of a NW with the shape shown in Fig. 2b but enlarged to a diameter of about 9.0 nm. In this process the ($\bar{1}$11) surfaces transformed into the most stable (001) surfaces leading to a sort of polycrystalline shape with four grains. These grains can be ideally obtained by reflections of one quarter of the cell shown by red lines in Fig. 2b and then by suitably scaling the system to a diameter of about 9 nm.

The final shape of the optimized NW with four twin boundaries at the center is shown in Fig. 3. This model consists of five replicas along the growth direction of a unit cell containing 3308 atoms with a lattice parameter along the growth axis of 16.93 Å. This supercell used to investigate the phase transitions thus contains $3308 \times 5 = 16540$ atoms (7980 Ge atoms and 8560 Te atoms). Note that only the (001) surfaces terminated by Te atoms and the mixed-terminated (1$\bar{1}$2) surfaces are now exposed. These reconstructions remove the net dipole moments present in the initial configuration (see Fig. 2b). The presence of twin boundaries at the center of the NW leads to a partial reconstruction giving rise to a sort of grain of α-GeTe with the c axis forming an angle of about 33.7° with the growth direction of the NW. The c axis of this grain lies in the plane formed by the growth direction of the NW and the direction indicated by x in Fig. 3. This misoriented grain contains 3200 atoms in the 16540-atom supercell. This particular shape is dictated by the very high surface-to-volume ratio in this ultrathin NW.

Note that the supercell lattice parameter along the growth direction has been set by using the theoretical equilibrium lattice parameters of crystalline α-GeTe reported in Table S1 in SI. The model has 3D periodic boundary conditions, the wire being infinite along the growth direction. The periodic images of the NW in the plane perpendicular to the growth direction are very far from each other (16 nm) and they do not intercat because of the short
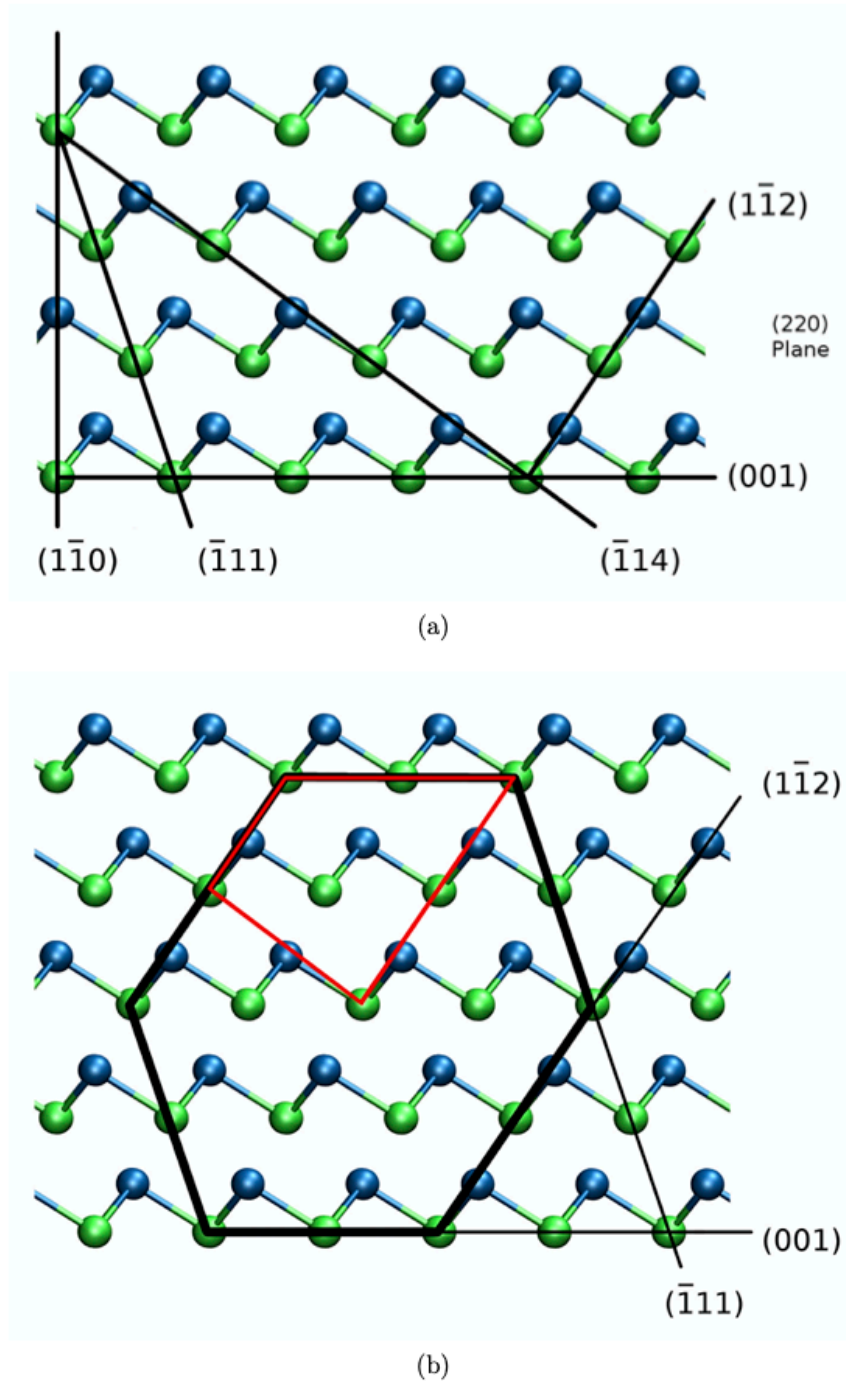
8

(a)

(b)

Figure 2: (a) Top view of the (220) plane of α-GeTe with several low index surfaces containing the [220] direction. (b) First guess for the section of the NW grown along the [220] direction. The actual starting geometry has been obtained by scaling the hexagonal shape to a diameter of about 9.0 nm. The part indicated by red lines can be used to generate a polycrystalline NW with four twin boundaries exposing only the (001) and (1$\bar{1}$2) surfaces (see Fig. 3).

range (cutoff radius of 6.879 Å) of the the NN interatomic potential. A file with the atomic positions and cell edges of the 3308-atom unit cell of the crystalline NW is given in the SI.

## Crystallization Kinetics of the Nanowires

To mimic the reset process in a PCM we liquefied a portion of the crystalline NW shown in Fig. 3 by keeping the rest of the atoms fixed in the crystalline positions as shown in Fig. 4. The liquid part was equilibrated for 30 ps at 1500 K. The supercell lattice parameter along the growth direction was also kept fixed. The system was then rapidly quenched below the melting temperature and equilibrated for 25 ps at 12 intermediate temperatures in the range 500-950 K, namely at 950, 900, 875, 850, 825, 800, 750, 700, 650, 600, 550, and 500 K. At this stage all the atoms of the model were free to move. At each temperature, we performed constant temperature simulations, 400 ps long, to study the kinetics of crystallization.

Firstly, we observed that at 850 K and above the crystalline part of the NW melts, while at 825 K and below the NW recrystallizes. We can conclude that the melting temperature of the NW is in the range 825-850 K. This value is sizably lower than the theoretical bulk melting temperature of 1001-1023 K computed from thermodynamic integration for the NN potential in Ref.[44] which is very close to the experimental value of 998 K.[55]

A reduction in T_m in NWs with respect to the bulk is expected in agreement with experimental findings.[21,28] However, since the NN potential used here is slightly different from that of Ref.,[44] we repeated the estimate of bulk T_m by repeating simulations similar to those performed for the NW. Namely, we built a slab geometry with a liquid part at high temperature in contact with a crystalline part initially frozen forming. The model is thus amde of two crystal/liquid interfaces periodically repeated in the direction perpendicular to the interface. Then we reduced the temperature by letting also the atoms in the crystalline part to move. Since the temperature is always above the α-β transition, the crystalline part was modeled in the β phase. We considered two different slab geometries exposing either the (100) or the (110) crystalline phase in contact with the liquid. Note that the (110) plane

10

(a)

1 nm
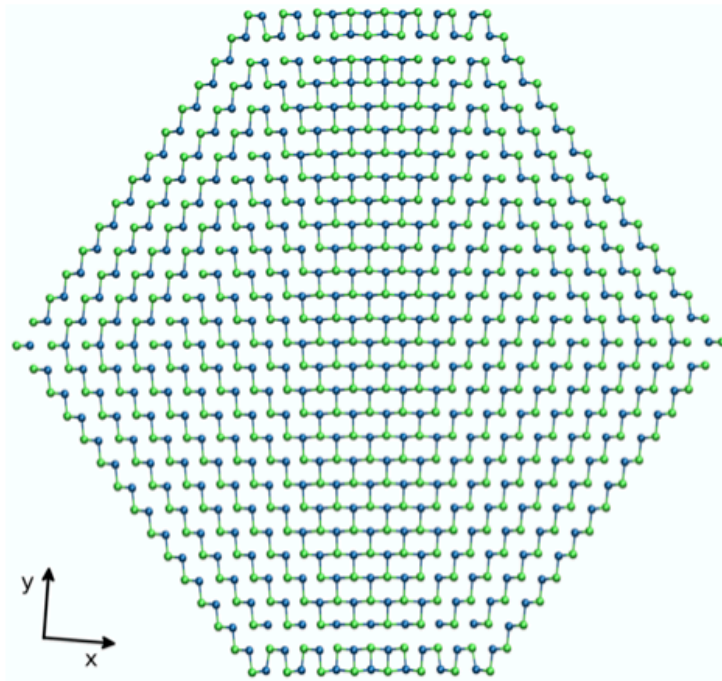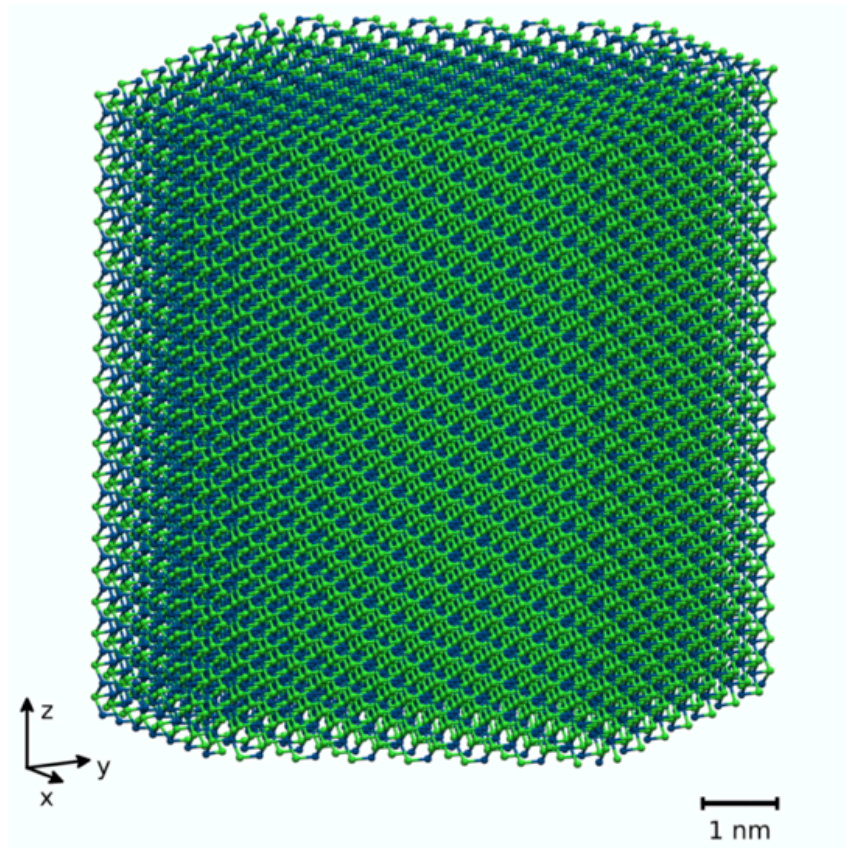
(b)

Figure 3: (a) Cross section and (b) side view of the GeTe NW used in the simulations. The nanowire has a hexagonal section with a diameter of about 9.0 nm.
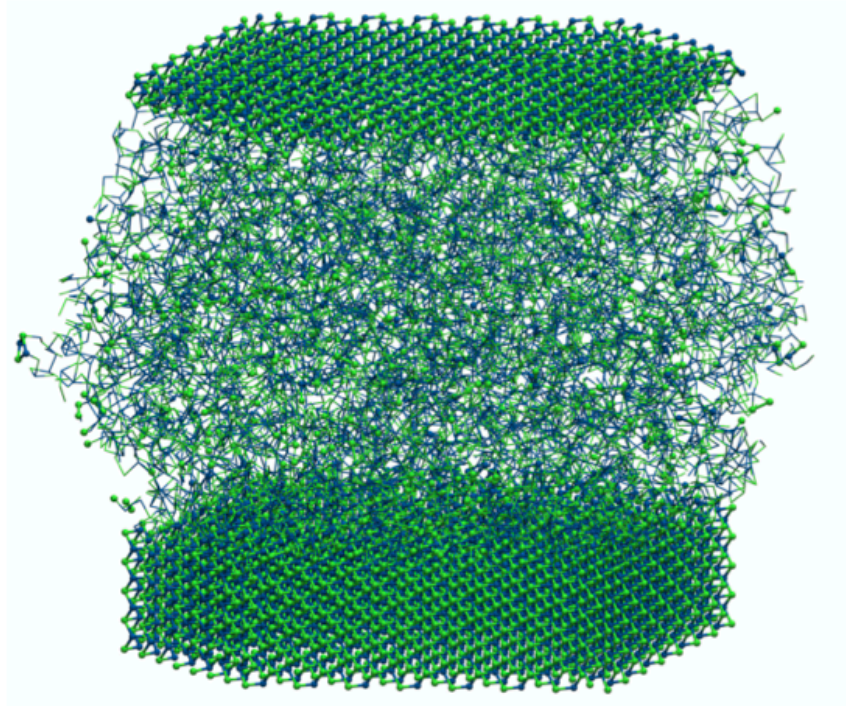
Figure 4: Snapshot of the liquefied portion of the GeTe NW in a 1500 K simulation where a part of the atoms has been kept fixed in the crystalline position.

of the cubic phase corresponds to the (110) plane of the α phase which is perpendicular to the [220] growth direction. This interface is therefore close to the liquid/crystal interface in our NW model. The slab used for these bulk-like simulations with the (110) interface is shown in Fig. 5, the corresponding figure for the (100) interface is given in Fig. S6 in SI. The supercell lattice parameters were set either by choosing the experimental density for the liquid phase[57] (see also Ref.[44]) and the equilibrium volume of the β phase. The latter was fixed to either that of the α phase computed from the NN potential, or to the experimental value of the β phase at the α-β transition (0.0369 at./Å^3),[58] supplemented by the thermal expansion with a linear expansion coefficient of $6.67 \cdot 10^{-5}$ K^{-1}.[59]

By looking at the movement of the liquid-crystalline interface we obtained a rough estimate of T_m because at temperatures below T_m the liquid crystallizes and the interface moves towards the liquid while at temperature above T_m a part of the crystalline region melts and the interface moves towards the crystal. In this way we estimated T_m to fall in the 900-925
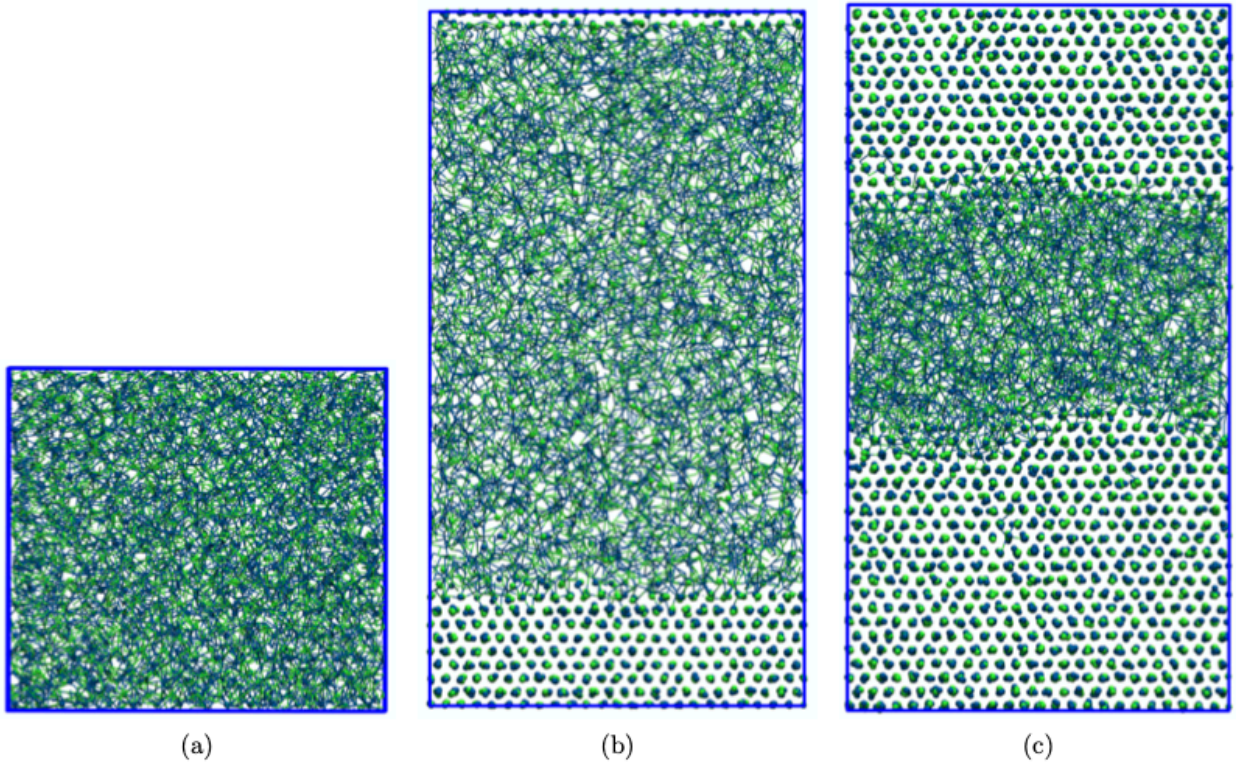
Figure 5: (a) Top view and (b) side view of the slab model used to estimate the melting temperature for the bulk in the initial configuration with the (110) surface of crystalline β-GeTe in contact with the liquid. (c) Snapshot after 300 ps of simulation at 700 K showing the crystallization of the liquid. Bonds are drawn only in the liquid region.

K range for both the (110) and (100) interfaces. The results do not change for the different choice of the equilibrium densities discussed above. We repeated the same simulations with the old NN potential of Ref.[44] which yielded T_m in the range 900-925 K for both the (100) and (110) interfaces. The melting temperature is therefore very similar for the two versions of the NN potential. We also repeated the simulations by including in the old and new NN potentials the van der Waals interaction according to Grimme[60] with the same parameters used in Ref.[44] with very similar bulk T_m in the range 900-925 K as well. The estimate of $T_m \sim 925$ K given here for the bulk is somehow lower than the result of the thermodynamic integration $T_m \sim 1001$-1023 K reported in Ref.[44] The reason for this discrepancy remains to be seen, but for the purpose of the present investigation the main outcome is that T_m for the bulk is about 100 K higher than for the ultrathin NW when estimated with the same procedure. The decrease in T_m in the NW with respect to the bulk is lower than in the experimental work of Ref.[21] where a melting temperature of 663 K has been reported for crystalline NWs 40-80 nm wide. The higher thermal stability of our model might be related to the choice of particularly stable crystalline surfaces which could be less abundant in the larger and rounded NWs grown experimentally.

We then analyzed the kinetics of recrystallization of the NW at temperatures below T_m. We did not observe crystal nucleation in the supercooled liquid but the growth of the crystal from the liquid/crystal interface. Snapshots of the crystallization of the NW at 700 K are shown in Fig. 6. To estimate the crystal growth velocity we proceeded as we did in Ref.[47] for the bulk crystallization at the liquid/crystal interface.

In order to assess whether an atom i belongs to the crystal or the liquid phase, we employed a variant of the order parameter for crystallinity introduced in Refs.[61–63] Namely, we used the averaged local order parameter $\bar{q}_{4m}(i)$ to build an order parameter $\bar{Q}_4(i)$ as

$$\bar{Q}_4(i) = \frac{1}{N_b(i)} \sum_{j=1}^{N_b(i)} \frac{\sum_m \bar{q}_{4m}(i)\bar{q}_{4m}(j)^*}{(\sum_m |\bar{q}_{4m}(i)|^2)^{1/2}(\sum_m |\bar{q}_{4m}(j)|^2)^{1/2}}$$

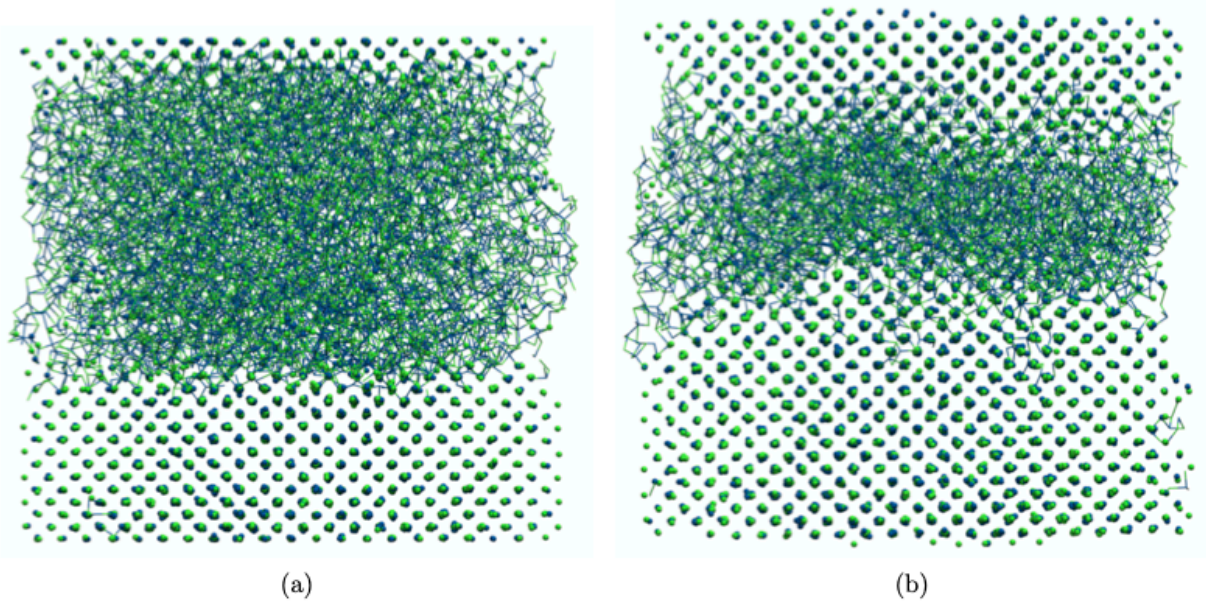(a)   (b)

Figure 6: Recrystallization of GeTe NW at 700 K. Model of the NW partially liquefied (left) and partially recrystallized after 300 ps (right). Bonds are drawn only in the liquid region.

$$\bar{q}_{4m}(i) = \frac{1}{\hat{N}_b(i)} \sum_{k=0}^{\hat{N}_b(i)} q_{4m}(k)$$

$$q_{4m}(k) = \frac{1}{N_b(k)} \sum_{l=1}^{N_b(k)} Y_{4m}(\hat{\mathbf{r}}_{kl}) \tag{1}$$

where j runs over the $N_b(i)$ neighboring atoms, k runs over the $\hat{N}_b(i)$ neighboring atoms including the i-th atoms itself, and $Y_{4m}(\hat{\mathbf{r}}_{kl})$ are the spherical harmonics of the polar angles defined by the versor $\hat{\mathbf{r}}_{kl}$ which links atoms k and l. The neighboring $N_b(i)$ atoms include the first coordination shell of crystalline GeTe at its theoretical equilibrium density. We define as crystalline an atom with $\bar{Q}_4$ greater than 0.9, and we consider two crystalline atoms connected when their distance is below 3.6 Å. This choice was shown to effectively discriminate the liquid from the crystalline nuclei in the simulations of GeTe crystallization in bulk in our previous work[47] which we refer to for further details.

We then defined an effective thickness of the crystalline part L_{cr} as defined by

$$L_{cr} = N_{cr} \cdot \frac{d_{hkl}}{2N_{surf}} \tag{2}$$

where N_{cr} is the number of crystalline atoms at time t, d_{hkl} is the spacing between (hkl) crystallographic planes, and N_{surf} is the number of atoms in a pristine crystalline surface layer. The factor 1/2 accounts for the fact that two crystal fronts are growing simultaneously from the two sides of the crystalline portion of the NW. In the NW simulations the liquid is in contact with the (110) plane (in the cubic notation which is equivalent to the (110) plane of the α-phase in the hexagonal notation, with the redundant index omitted). The d_{110} spacing is $\sim$ 2.11 Å and depends very little on temperature. The speed of crystal growth u is then obtained from the slope of L_{cr} as a function of time. Examples of the time evolution of L_{cr} in the NW at two different temperatures are given in Fig. 7. The corresponding plot for the other temperatures is given in Fig. S7 in SI.

The same analysis was repeated for the bulk-like crystallization in the slab geometry used to estimate bulk T_m described above. The resulting crystal growth velocities for the NW and for the bulk at the (110) liquid/crystal interface are reported in Fig. 8 as a function of temperature. The crystal growth velocity at the liquid/crystal (110) interface in bulk GeTe is similar to the values obtained previously at 500 K and 700 K for the (111) and (100) interface in Ref.[47]

In our previous works[46,47] we have shown that the crystal growth velocity for supercritical nuclei in the supercooled liquid and at the crystal-liquid interface in slab models can be described by the expression for classical nucleation theory (CNT)[64]

$$u = \frac{4D}{\lambda}(1 - exp(-\Delta\mu/k_BT))exp(\Delta\mu/2k_BT) \tag{3}$$

where D is the diffusion coefficient and $\Delta\mu$ is the difference in free energy between the liquid and crystalline phases and λ is a typical jumping distance. The last exponential factor in Eq. 3 was omitted in Refs.[46,47] which is a good approximation close to T_m. The last
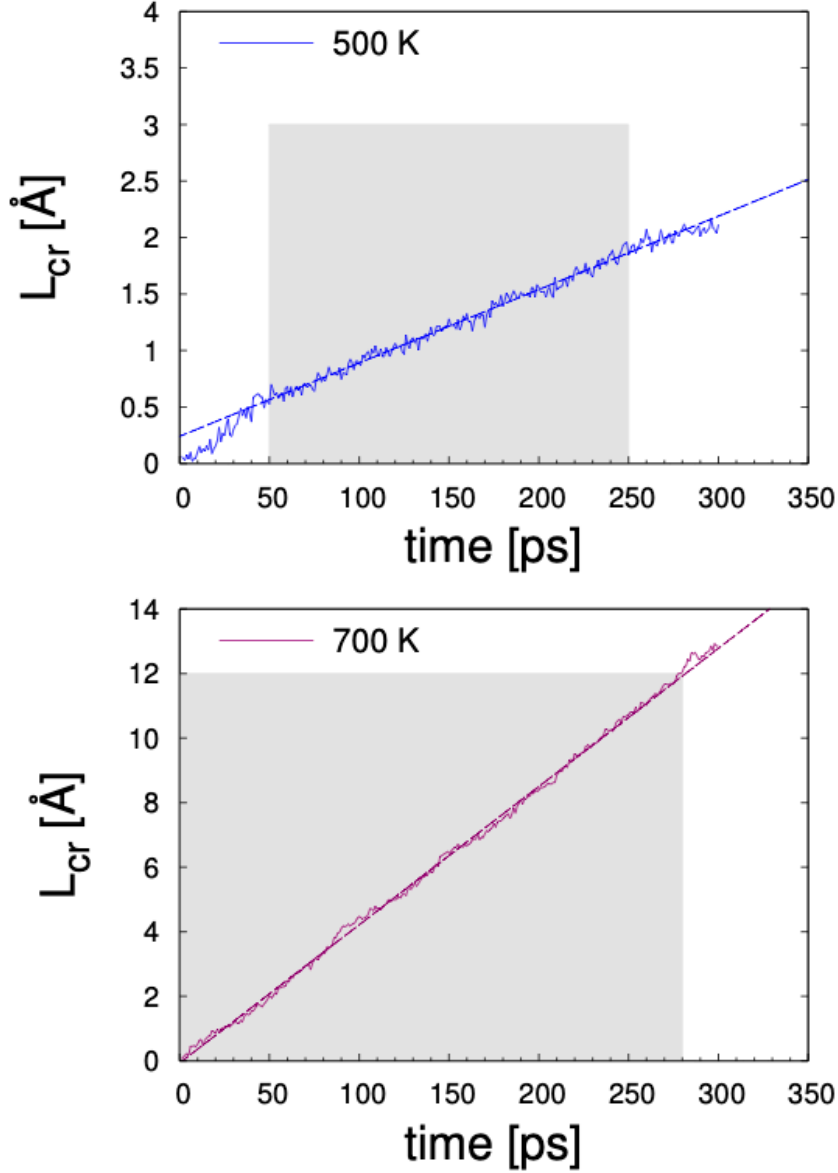
Figure 7: Linear dimension of the crystal growth front ($L_{cr}(t)$ $L_{cr}(t_0)$, see text) as a function of time in the NW at 500 K and 700 K. The shaded area indicate the interval used to define the slope of the curves which corresponds to the crystal growth velocity.

exponential term enhances the crystal growth velocity at lower temperatures and removing this term actually leads to a better fitting of our simulation data. For the sake of consistency this term is, however, kept in the fitting procedure described below.

The highest crystal growth velocity of about 8 m/s at the crystal/liquid interface in bulk shown in Fig. 8 occurs at about 750 K. This value is lower than the corresponding estimate
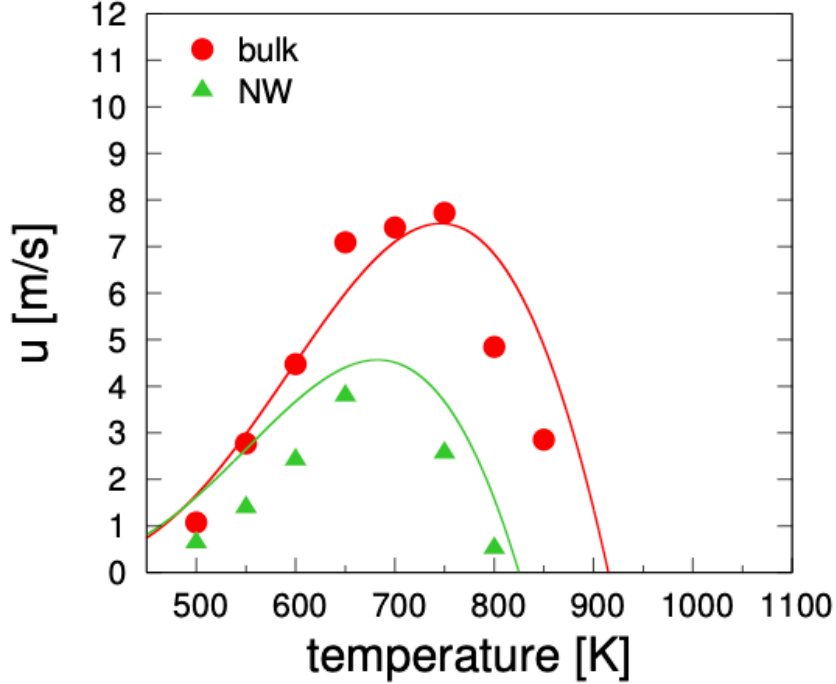
17

Figure 8: Crystal growth velocity u for the NW (green triangle) and the (110) crystal/liquid interface in the bulk (red dots, see text). The continous lines are the result of the fitting with Eqs. 3 and and 4.

of about 800 K given in Ref.[46] on the basis of the extrapolation with CNT of simulations data below 650 K. This discrepancy is, however, in line with the melting temperature of about 925 K reported here which differs from the value of 1001-1023 K used in the extrapolation procedure of Ref.[46] Time resolved electron diffraction measurements on laser-induced crystallization of bulk GeTe yielded a maximum crystal growth velocity of about 3.3 m/s at 850 K.[65]

The lower crystal growth velocity in the NW with respect to the bulk (see Fig. 8) can be ascribed to the lower T_m of the NW which leads to a lower thermodynamical driving force for the crystallization $\Delta\mu$ at a given temperature in the NW with respect to the bulk as discussed below. The data on the crystal growth velocity for the bulk and NW can actually can be satisfactorely reproduced by Eq. 3. Because of the presence of the free surfaces and of the interface with the crystal the atomic mobility is inhomogeneous in the partially molten NW. We therefore used in Eq. 3 the temperature dependent diffusion coefficient calculated for

18

the homogeneous bulk in our previous work[44] ($D = D_o \exp(-E_a/k_B T)$, with $D_o = 1.2 \cdot 10^{-3}$ cm^2/s and $E_a = 0.296$ eV). We set $\lambda = 3$ Å and we used the Thomson-Spaepen[66] formula for the temperature dependent driving force $\Delta\mu$, namely

$$\Delta\mu = \frac{\Delta H_f}{T_m}\frac{2T(T_m - T)}{(T_m + T)} - (T_m - T)^2 A\left(\frac{1}{2} - \frac{T_m}{T_m + T}\right) \tag{4}$$

where ΔH_f is the latent heat of fusion, and the parameter A is defined by the approximated value for the difference in the specific heat at constant pressure between the liquid and solid written as $\Delta C_P = \frac{\Delta H_f}{T_m} + A(T - T_m)$. The value $\Delta H_f = 0.186$ eV/atom for the bulk was obtained from NN simulations in our previous work.[44] For the NW we have scaled ΔH_f by the ratio T_m^{NW}/T_m^{bulk} under the assumption that the entropy of fusion is the same in the bulk and NW. We have taken A as a fitting parameter for the crystal growth velocities in the bulk which yielded $A = -7.13 \cdot 10^{-7}$ eV/atom/K^2. This value is within the range of values obtained for different classes of materials in Ref.[66] . As a first approximation the same value for A was taken for the NW. According to the discussion reported above, we have taken $T_m = 915$ K for the bulk and $T_m = 825$ K for the NW. The analytic curves for the crystal growth velocities of bulk and NW, obtained from Eqs. 3 and 4 with the parameters given above, are shown in Fig. 8. The agreement with the actual values of the crystal growth velocities extracted from the simulations is only qualitative, but overall satisfactorily, considering the uncertainties in the approximations and parameters involved. These results suggest that the difference in the crystal growth velocities between the NW and the bulk can be mostly accounted for by the different melting temperatures.

Structural relaxations and resistance drift in nanowires

The metastable amorphous state of phase change materials is subject to aging which leads to an increase in the electrical resistivity with time. This phenomenon called drift[32] is described by a power law function $R = R_o(t/t_o)^\nu$ where R and R_o are the resistance at

time t and t_o and ν is the drift exponent. The drift should be kept as low as possible as it affects the reliability of the devices and it hinders the realization of multilevel cells.[33] Optical ellipsometry measurements of the prototypical compound $Ge_2Sb_2Te_5$ upon drift have shown a widening of the band gap and a reduction of Urbach tails.[67]

By means of combined molecular dynamics simulations and electronic structure calculations based on DFT, in a previous work[36] we found that the resistance drift in the prototypical phase change compound GeTe can be ascribed to the removal of chains of Ge-Ge homopolar bonds. These structural relaxations lead to both an increase of the Tauc optical gap and to a reduction of the Urbach tails.

We briefly summarize the results of our previous work on bulk GeTe[36] before addressing the same issue in NW. Models of a-GeTe 1728-atom large were generated in Ref.[36] by quenching from the melt within NN-MD simulations. The structure of amorphous models were then relaxed by DFT-PBE simulations with the CP2k suite of programs.[68] In order to study the Ubach tails and the defect states in the gap, the Kohn-Sham energies were then computed with the exchange-correlation potential proposed by Engel and Vosko (EV)[69] and with the self-consistent electronic density at the PBE level. This functional is known to better reproduce the band gap and it is less computationally demanding than the hybrid functional used previously with small models.[70]

The analysis of the electronic structure revealed the presence of a broad distribution of localized states in the gap and at the band edges. A clear correlation was found between these localized electronic states and the presence of short chains of Ge-Ge homopolar bonds. Homopolar Ge-Ge bonds are indeed abundant in a-GeTe. In the models of Ref.[36] about 72 % of Ge atoms forms at least one bond with another Ge atom. About 48.5 % of Ge atoms belongs to Ge-Ge chains containing four or more Ge atoms. These Ge-Ge chains are not an artifact of the NN potential as a similar distribution of Ge-Ge chains was found in ten 216-atom models of a-GeTe generated either by NN or by full DFT-PBE simulations. These chains of Ge-Ge bonds are not isolated from the rest of the amorphous network, Ge atoms

20

belonging to the chains are mostly four-fold coordinated and bonded with Te atoms as well.

We then envisaged that the removal of these Ge-Ge chains would lead to a reduction of the in-gap states and to a widening of the band gap. To check this idea we removed part of these chains by metadynamics simulations[71] at 300 K. This technique allows breaking the Ge-Ge bonds in an affordable simulation time even at lower temperatures where atomic mobility is low and crystal nucleation does not occur. Annealing at 500 K leads instead to partial crystallization on the time scale of few hundreds ps.[46] The metadynamics method[71] is based on a coarse-grained, non- Markovian dynamics in the manifold spanned by few reaction coordinates (collective variables), biased by a history-dependent potential, which drives the system towards the lowest saddle point. In our case, we chose two collective variables defined by the partial coordination numbers Ge-Ge and Ge-Te for atoms in Ge-Ge chains. After metadynamics simulations 4 ns long, the geometry of the resulting model was optimized at the DFT-PBE level. The final configuration was about 10.8 eV (1728-atom) lower in energy than the initial one optimized at DFT-PBE level before the metadynamics was applied. In the final state after metadynamics, the fraction of Ge atoms in chains containing more than four Ge atoms was reduced from 48.5 % (before metadynamics) to 39.6 %.

The decrease in the number of Ge-Ge chains actually leads to a reduction of Urbach tails and of the states in the gap and to an enhancement of their localization. A widening of the band gap was also observed as quantified by the Tauc optical gap. This is defined as the energy E for which the linear extrapolation of the function $E\sqrt{\epsilon_2(E)}$ becomes zero, where $\epsilon_2(E)$ is the imaginary part of the dielectric function computed from the Kubo-Greenwood formula as we did previously for GeTe and other chalcogenide compounds.[72] After metadynamics simulations the Tauc optical gap increased by about 20 meV that is even quantitatively close to the increase of the Tauc gap by 40 meV measured experimentally in $Ge_2Sb_2Te_5$ upon drift.[67]

In the a-GeTe models, a fraction of about 30 % of Ge atoms is in tetrahedral configuration

21

while the rest of atoms are in defective octahedral (4- or 5-fold coordinated) or pyramidal (3-fold coordinated) configurations.[36,38] The decrease in the fraction of Ge-Ge bonds due to the removal of Ge-Ge chains also leads to a reduction of tetrahedra which are favored by homopolar bonds, as indeed revealed by recent XANES measurements.[73] The area of the XANES feature associated with tetrahedra decreases by at most 10 % upon drift which means that this change involves about 3 % of Ge atoms. After metadynamics the fraction of tetrahedral Ge atoms decreases from 32 % to 30 % of the total number of Ge atoms which is a reduction even quantitatively consistent with the XANES data.[73]

In a recent DFT study of 216-atom models,[74] the reduction of tetrahedra was actually proposed as the main source of the resistance drift in a-GeTe.[74] In our simulations the reduction of tetrahedra was much lower than the reduction in the number of Ge atoms in longer Ge-Ge chains responsible for the states in the gap and at the band edges. We therefore suggested that the reduction of tetrahedra is a side effect of the removal of chains of Ge-Ge bonds. We remark that similar chains of wrong bonds (Ge-Ge, Ge-Sb and Sb-Sb) are present also in DFT models of a-$Ge_2Sb_2Te_5$.[76] Chains of Sb-Sb bonds are also found in the DFT model of amorphous Sb_2Te_3 of Ref.,[77] which would suggest a similar origin for the drift in a-Sb_2Te_3 which lacks tetrahedral Ge sites. The removal of homopolar (wrong) bonds might be a common feature of the resistance drift in GeSbTe alloys.

A statistical analysis of the DFT electronic structure of several small 216-atom models of a-GeTe generated with a Tersoff-like potential[78] also confirmed that the removal of homopolar bonds lead to a bleaching of band gap states. In this latter work, however, the drift is not ascribed to a widening of the band gap but to a shift of the Fermi level towards midgap upon aging. This conclusion seems at odds with more recent experimental data on GeTe and $Ge_2Sb_2Te_5$ that show a strict correlation between the activation energy for conduction and the optical band gap upon drift which implies a negligible shift of the Fermi level.[75]

On the basis on the analysis of the drift in bulk GeTe summarized above, we have analyzed the structure of a model of an amorphized NW. Once a part of the NW was melt

as described in Sec. IIIB, the temperature was rapidly decreased to 300 K in about 100 ps. This procedure leads to the formation of an amorphous section containing about 4700 Ge atoms shown in Fig. 9. A file with the atomic positions and cell edges of the 16540-atom partially amorphized NW is given in the SI.
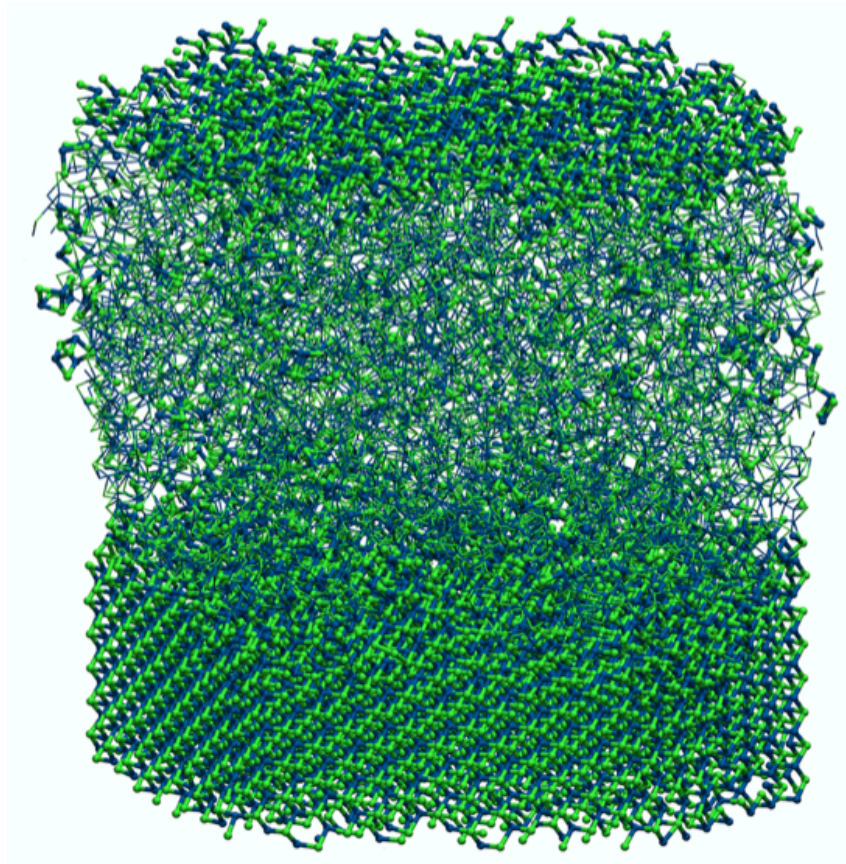

Figure 9: Snapshot of the amorphized part of the GeTe NW.

The fraction of Ge atoms that form at least one homopolar bond is about 60 % similarly in the NW and in a bulk model of a-GeTe generated with the same protocol (4096-atom). However, while in the bulk a fraction of 33 % of Ge atoms are within Ge-Ge chains containing more than four Ge atoms (in models generated with the new NN potential used here), in the NW this fraction reduced to 26 %. Although it might seem just a tiny change we remark that a reduction of about 10 % of the fraction of Ge atoms involved in longer chains (≥ 4 Ge atoms) was sufficient to sizably clean the in-gap states and widen the band gap in the
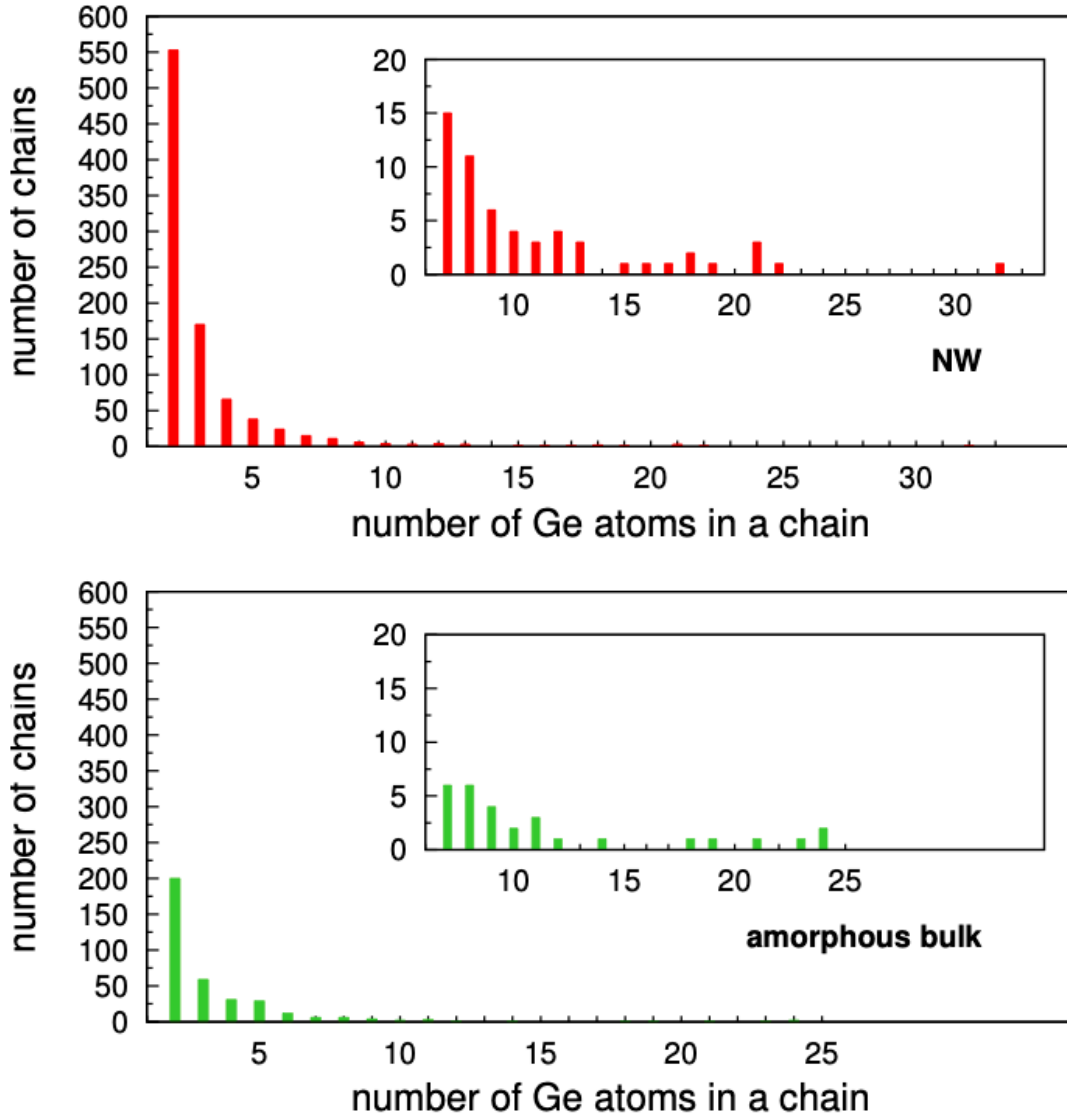
metadynamics simulations of Ref.[36]

Figure 10: Distribution of the number of chains of Ge-Ge bonds as a function of the number (≥ 4) of atoms in the (also branched) chain in the amorphous part of a mixed crystalline/amorphous GeTe NW (upper panel) and in a bulk model of a-GeTe. There are 4722 Ge atoms in the amorphous part of the NW and 2048 Ge atoms in the bulk model. The inset is a magnification of the distribution of long chains.

The distribution of the Ge-Ge chains in the NW and in a bulk model of a-GeTe are reported in Fig. 10. The bulk model 4096-atom large was generated by quenching from the melt following the same protocol used in Ref.[36] The distribution of Ge-Ge chains refer to

the model optimized with the NN potential only (the same used for the NW) while in the analysis of Ref.[36] the 1728-atom a-GeTe model generated with the NN potential was further relaxed at the DFT level. The absolute number of Ge-Ge chains is larger in the NW than in the bulk because of the larger number of Ge atoms (4722 in the amorphous part of the NW and 2048 in the bulk), but the fraction of Ge atoms beloging to the Ge-Ge chains is lower in the NW than in the bulk as discussed above. The presence of the free surfaces in the NW somehow favors a better structural relaxation during the reset process that leads to a more stable amorphous state with a lower fraction of longer Ge-Ge chains. This feature could explain the mitigation of the drift phenomenon in GST NW observed experimentally.[31]

Conclusions

We have performed large scale atomistic simulations on the crystallization kinetics of GeTe nanowires by using an interatomic potential based on the fitting of a large DFT database by means of a Neural Network scheme. The model of an ultrathin NW with diameter of about 9 nm was generated by choosing the [220] growth direction detected experimentally in several NWs synthesized via the vapor-liquid-solid process. The shape of the NW was chosen in order to expose the most stable crystalline surfaces. The simulations revealed that the melting temperature is lower by about 100 K in the NW with respect to the bulk as estimated from the coexistence of the crystal/liquid interface. The crystallization speed is consistently lower than in the bulk by about a factor two mostly because of the reduced T_m which implies a lower thermodynamical driving force for crystallization. This overall small reduction in the crystallization speed with respect to the bulk makes the NW attractive for applications in PCM as suggested in several previous experimental works on GeTe and other materials in the same class. The analysis of the amorphous NW generated by quenching from the melt revealed a lower fraction of chains of homopolar bonds with respect to the bulk. These latter structures are subject to aging with time and they have been identified in our previous work as the source of resistance drift in the amorphous phase of the bulk.

A lower fraction of these structures could be the source of a mitigated drift phenomenon in the NW reported experimentally. However, other mechanisms can be at hand to reduce the drift in NW once the amorphization is obtained without melting such as for instance by migration and jamming of dislocations as proposed in Ref.[29,30]

Acknowledgement

Supporting Information

Snapshot and structural properties of a small amorphous nanowire from neural network and DFT simulations, pair correlation functions of bulk amorphous and liquid GeTe obtained with the new neural network potential, snapshots of models used to estimate the bulk melting temperature, plots of the data used to compute the crystal growth velocity, table of the lattice parameters of crystalline α-GeTe obtained with the neural network potential, file xyz of the atomic positions and cell edges of the 3308-atom model of crystalline nanowire, file xyz of the atomic positions and cell edges of the 16540-atom model of partially amorphized nanowire.

References

(1) Burr, G. W.; Kurdi, B. N.; Scott, J. C.; Lam, C. H.; Gopalakrishnan, K.; R. S. Shenoy, R. S. Overview of Candidate Device Technologies for Storage-Class Memory. *IBM J. Res. Dev.* **2008**, *52*, 449-464.

(2) Wuttig, M.; Yamada, N. Phase-Change materials for Rewriteable Data Storage. *Nat. Mater.* **2007**, *6*, 824-832.

(3) Pirovano, A.; Lacaita, A. L.; Benvenuti, A.; Pellizzer, F.; Bez, R. Electronic Switching in Phase-Change Memories. *IEEE Trans. Electron. Dev.* **2004**, *51*, 452-459.

(4) Lacaita, A. L.; Wouters, D. J. Phase-Change Memories. *Phys. Stat. Sol. A* **2008**, *205*, 2281-2297.

(5) Lencer, D.; Salinga, M.; Wuttig, M. Design Rules for Phase-change Materials in Data Storage Applications. *Adv. Mat.* **2011**, *23*, 2030-2058.

(6) Raoux, S.; Welnic, W.; Ielmini, D. Phase Change Materials and Their Application to Nonvolatile Memories. *Chem. Rev.* **2010**, *110*, 240-267.

(7) Lee, S.-H.; Jung, Y.; Agarwal, R. Highly Scalable Non-Volatile and Ultra-Lowpower Phase-change Nanowire Memory. *Nat. Nanotech.* **2007**, *2*, 626-630.

(8) Piccione, B.; Agarwal, R.; Jung, Y.; Agarwal, R. Size-Dependent Chemical Transformation, Structural Phase Change, and Optical Properties of Nanowires. *Phil. Mag.* **2013**, *93*, 2089-2121.

(9) Lee, S.-H.; Jung Y.; Agarwal R. Size-Dependent Surface-Induced Heterogeneous Nucleation Driven Phase-Change in $Ge_2Sb_2Te_5$ Nanowires. *Nano Lett.* **2008**, *8*, 3303-3309.

(10) Jung, Y.; Lee, S.-H.; Ko, D.-K.; Agarwal, R. Synthesis and Characterization of $Ge_2Sb_2Te_5$ Nanowires with Memory Switching Effect. *J. Am. Chem. Soc.* **2006**, *128*, 14026-14027.

(11) Longo, M.; Fallica, R.; Wiemer, C.; Salicio, O.; Fanciulli, M.; Rotunno, E.; Lazzarini, L. Metal Organic Chemical Vapor Deposition of Phase Change $Ge_1Sb_2Te_4$ Nanowires. *Nano Lett.* **2012**, *12*, 1509-1515.

(12) Jung, C. S.; Kim, H. S.; Im, H. S.; Seo, Y. S.; Park, K.; Back, S. H.; Cho, Y. J.; Kim, C. H.; Park, J.; Ahn, J.-P. Polymorphism of GeSbTe Superlattice Nanowires. *Nano Lett.* **2013**, *13*, 543-549.

(13) Lee, S.-H.; Jung, Y.; Chung, H.; Jennings, A. T.; Agarwal, R. Comparative Study of Memory-Switching Phenomena in Phase Change GeTe and $Ge_2Sb_2Te_5$ Nanowire Devices. *Physica E* **2008**, *40*, 2474-2480.

(14) Jung, Y.; Yang, C.-Y.; Lee, S.-H.; Agarwal, R. Phase-Change Ge-Sb Nanowires: Synthesis, Memory Switching, and Phase-Instability. *Nano Lett.* **2008**, *9*, 2103-2108.

(15) Meister, S.; Peng, H.; McIlwrath, K.; Jarusch, K.; Zhang X. F.; Cui, Y. Synthesis and Characterization of Phase-Change Nanowires. *Nano Lett.* **2006**, *6*, 1514-1517.

(16) Zuev, Y. M.; Lee, J. S.; Galloy, C.; Park, H.; Kim, P. Diameter Dependence of the Transport Properties of Antimony Telluride Nanowires. *Nano Lett.* **2010**, *10*, 3037-3040.

(17) Rotunno, E.; Longo, M.; Wiemer, C.; Fallica, R.; Campi, D.; Bernasconi, M.; Lupini, A. R.; Pennycook, S. J.; Lazzarini, L. A Novel Sb_2Te_3 Polymorph Stable at the Nanoscale. *Chemistry of Materials* **2015**, *27*, 4368-4373.

(18) Lee, S.-H.; Ko, D.-K.; Jung, Y.; Agarwal, R. Size-Dependent Phase Transition Memory Switching Behavior and Low Writing Currents in GeTe Nanowires. *Appl. Phys. Lett.* **2006**, *89*, 223116.

(19) Yu, D.; Wu, J.; Gu, Q.; Park, H. Germanium Telluride Banowires and Nanohelices with Memory-Switching Behavior. *J. Am. Chem. Soc.* **2006**, *128*, 8148-8149.

28

(20) Yim, J. W. L.; Xiang, B.; Wu, J. Sublimation of GeTe Nanowires and Evidence of Its Size Effect Studied by in Situ TEM. *J. Am. Chem. Soc.* **2009**, *131*, 14526-14530.

(21) Sun, X.; Yu, B.; Ng, G.; Meyyappan, M. One-dimensional Phase-Change Nanostructure: Germanium Telluride Nanowire. *J. Phys. Chem. C* **2007**, *111*, 2421-2425.

(22) Longo, M.; Wiemer, C.; Salicio, O.; Fanciulli, M.; Lazzarini, L.; Rotunno, E. Au-Catalyzed Self Assembly of GeTe Nanowires by MOCVD. *J. Cryst. Growth* **2011**, *315*, 152-156.

(23) Jennings, A. T.; Jung, Y.; Engel, J.; Agarwal, R. Diameter-Controlled Synthesis of Phase-Change Germanium Telluride Nanowires via the Vapor-Liquid-Solid Mechanism. *J. Phys. Chem. C* **2009**, *113*, 6898-6901.

(24) Chung, H.-S.; Jung, Y.; Kim, S. C.; Kim, D.-H.; Oh, K.H.; Agarwal, R. Epitaxial Growth and Ordering of GeTe Nanowires on Microcrystals Determined by Surface Energy Minimization. *Nano Lett.* **2009**, *9*, 2395-2401.

(25) Selmo, S.; Cecchi, S.; Cecchini, R.; Wiemer, C.; Fanciulli, M.; Rotunno, E.; Lazzarini, L.; Longo, M. MOCVD Growth and Structural Characterization of In-Sb-Te Nanowires. *Phys. Status Solidi A* **2016**, *213*, 335-338.

(26) Jung, Y.; Lee, S.-H.; Jennings, A. T.; Agarwal, R. Core-Shell Heterostructured Phase Change Nanowire Multistate Memory. *Nano Lett.* **2008**, *8*, 2056-2072.

(27) Lee, J. S.; Brittman, S.; Yu, D.; Park, H. Vapor-Liquid-Solid and Vapor-Solid Growth of Phase-Change Sb_2Te_3 Nanowires and Sb_2Te_3/GeTe Nanowire Heterostructures. *J. Amer. Chem. Soc.* **2008**, *130*, 6252-6258.

(28) Sun, X. H.; Yu, B.; Ng, G.; Nguyen, T. D.; Meyyappan, M. III-VI Compound Semiconductor Indium Selenide (In_2Se_3) Nanowires: Synthesis and Characterization. *Appl. Phys. Lett.* **2006**, *89*, 233121.

(29) Nam, S.-W.; Chung, H.-S.; Lo, Y. C.; Qi, L.; Li, J.; Lu, Y.; Johnskn, A. T. C.; Jung, Y.; Nukala, P.; Agarwal, R. Electrical Wind Force-Driven and Dislocation-Templated Amorphization in Phase-Change Nanowires. *Science* **2012**, *336*, 1561-1566.

(30) Nukala, P.; Lin, C.-C.; Composto, R.; Agarwal, R. Ultralow-Power Switching via Defect Engineering in Germanium Telluride Phase-Change Memory Devices. *Nat. Comm.* **2016** *7*, 10482.

(31) Mitra, M.; Jung, Y.; Gianola, D. S.; Agarwal, R. Extremely Low Drift of Resistance and Threshold Voltage in Amorphous Phase Change Nanowire Devices. *Appl. Phys. Lett.* **2010** *96*, 222111.

(32) Pirovano, A.; Lacaita, A. L.; Pellizzer, F.; Kostylev, S. A.; Benvenuti, A.; Bez, R. Low-Field Amorphous State Resistance and Threshold Voltage Drift in Chalcogenide Materials. *IEEE Trans. Electron. Devices* **2004**, *51*, 714-719; Ielmini, D.; Lacaita, A. L.; Mantegazza, D. Recovery and Drift Dynamics of Resistance and Threshold Voltages in Phase-Change Memories. *IEEE Trans. Electron. Devices* **2007**, *54*, 308-315.

(33) Sebastian, A.; Papandreou, N.; Pantazi, A.; Pozidiz, H.; Eleftheriou, E. Non-Resistance-Based Cell-State Metric for Phase-Change Memory. *J. Appl. Phys.* **2011**, *110*, 084505.

(34) Sosso, G. C.; Miceli, G.; Caravati, S.; Behler, J.; Bernasconi, M. Neural Network Interatomic Potential for the Phase Change Material GeTe. *Phys. Rev. B* **2012**, *85*, 174103.

(35) Behler, J.; Parrinello, M. Generalized Neural-Network Representation of High-Dimensional Potential-Energy Surfaces. *Phys. Rev. Lett.* **2007**, *98*, 146401; Behler, J. Atom-centered Symmetry Functions for Constructing High-Dimensional Neural Network Potentials. *J. Chem. Phys.* **2011**, *134*, 074106; J. Behler, Angew. Chemie, in press (2017), DOI: 10.1002/anie.201703114.

(36) Gabardi, S.; Caravati, S.; Sosso, G. C.; Behler, J.; Bernasconi, M. Microscopic origin of Resistance Drift in the Amorphous State of the Phase-Change Compound GeTe. *Phys. Rev. B* **2015**, *92*, 054201.

(37) Perdew, J.P.; Burke, K.; Ernzerhof, M. Generalized Gradient Approximation Made Simple. *Phys. Rev. Lett.* **1996**, *77*, 3865-3868.

(38) Mazzarello, R.; Caravati, S.; Angioletti-Uberti, S.; Bernasconi, Parrinello, M. Signature of Tetrahedral Ge in the Raman Spectrum of Amorphous Phase-Change Materials. *Phys. Rev. Lett.* **2010**, *104*, 085503; erratum **2011**, *107*, 039902.

(39) Caravati, S.; Bernasconi, M.; Kühne, T. D.; Krack, M. Parrinello, M. Coexistence of Tetrahedral- and Octahedral-Like Sites in Amorphous Phase Change Materials. *Appl. Phys. Lett.* **2007**, *91*, 171906.

(40) Akola, J.; Jones, R. O. Structural Phase Transitions on the Nanoscale: The Crucial Pattern in the Phase-Change Materials $Ge_2Sb_2Te_5$ and GeTe. *Phys. Rev. B* **2007**, *76*, 235201.

(41) Hegedüs, J.; Elliott, S. R. Microscopic Origin of the Fast Crystallization Ability of Ge-Sb-Te Phase-Change Memory Materials. *Nat. Mater.* **2008**, *7*, 399-405.

(42) Sosso, G. C.; Donadio, D.; Caravati, S.; Behler, J.; Bernasconi, M. Thermal Transport in Phase-Change Materials from Atomistic Simulations. *Phys. Rev. B* **2012**, *86*, 104301.

(43) Campi, D.; Donadio, D.; Sosso, G. C.; Behler, J.; Bernasconi, M. Electron-Phonon Interaction and Thermal Boundary Resistance at the Crystal-Amorphous Interface of the Phase Change Compound GeTe. *J. Appl. Phys.* **2015**, *117*, 015304.

(44) Sosso, G.C.; Behler, J.; Bernasconi, M. Breakdown of Stokes-Einstein Relation in the Supercooled Liquid State of Phase Change Materials. *Physica Status Solidi B* **2012**, *249*, 1880-1885; erratum **2013**, *250*, 1453.

(45) Sosso, G. C.; Behler, J.; Bernasconi, M. Atomic Mobility in the Overheated Amorphous GeTe Compound for Phase Change Memories. *Physica Status Solidi A* **2016**, *213*, 329-334.

(46) Sosso, G. C.; Miceli, G.; Caravati, S.; Behler, J.; Bernasconi, M. Fast Crystallization of the Phase Change Compound GeTe by Large-Scale Molecular Dynamics Simulations. *J. Phys. Chem. Lett.* **2013**, *4*, 4241-4246; Sosso, G. C.; Colombo, J.; Del Gado, E.; Behler, J.; Bernasconi, M. Dynamical Heterogeneity in the Supercooled Liquid State of the Phase Change Material GeTe. *J. Phys. Chem. B* **2014**, *118*, 13621-13628.

(47) Sosso, G. C.; Salvalaglio, M.; Behler, J.; Bernasconi, M.; Parrinello, M. Heterogeneous Crystallization of the Phase Change Material GeTe via Atomistic Simulations. *J. Phys. Chem. C* **2015**, *119*, 6428-6434.

(48) RuNNer: A Neural Network Code for High-Dimensional Potential-Energy Surfaces, Jörg Behler, Institut für Physikalische Chemie, Universität Göttingen, Germany.

(49) Smith, W.; Forester, T. R. DL_POLY_2.0: A General-Purpose parallel Molecular Dynamics Simulation Package. *J. Mol. Graph.* **1996**, *14*, 136-141.

(50) Bussi, G.; Donadio, D.; Parrinello, M. Canonical Sampling Through Velocity Rescaling. *J. Chem. Phys.* **2007**, *126*, 01410.

(51) Goldak, J.; Barrett, C. S.; Innes, D.; Youdelis, W. Structure of α-GeTe. *J. Chem. Phys.* **1966**, *44*, 3323-3325.

(52) Chattopadhyay, T.; Boucherle, J.; Von Schnering, H. Neutron-Diffraction Study on the Structural Phase-Transition in GeTe. *J. Phys. C* **1987**, *20*, 1431-1440.

(53) Fons, P.; Kolobov, A. V.; Krbal, M.; Tominaga, J.; Andrikopoulos, K. S.; Yannopoulos, S. N.; Voyiatzis, Uruga, T. Phase Transition in Crystalline GeTe: Pitfalls of Averaging Effects. *Phys. Rev. B* **2010**, *82*, 155209.

(54) Matsunaga, T.; Fons, P.; Kolobov, A. V.; Tominaga, J.; Yamada, N. The Order-Disorder Transition in GeTe: Views from Different Length-Scales. *Appl. Phys. Lett.* **2011**, *99*, 231907.

(55) Klemm, W.; Frischmuth, G. Das System Germanium-Tellur. *Z. Anorg. Chem.* **1934**, *218*, 249-251.

(56) Deringer, V. L.; Lumeij, M.; Dronskowski, R. Ab Initio Modeling of α-GeTe(111) Surfaces. *J. Phys. Chem. C* **2012**, *116*, 15801-15811.

(57) Glazov, V. M.; Shchelikov, O. D. Thermal-Expansion and Characteristics of the Atomic Bond Strength in Melts of IV-VI Compounds (AIV = Ge, Sn, Pb - BVI = S, Se, Te). *Sov. Phys. Semicond.* **1984**, *18*, 411-413.

(58) Wiedemeier, H.; Siemers, P. A. The Thermal Expansion of GeS and GeTe *J. Less-Common Met.* **1989**, *146*, 279-298.

(59) Chatterji, T.; Kumar, C. M. N.; Wdowik, U. D. Anomalous Temperature-Induced Volume Contraction in GeTe *Phys. Rev. B* **2015**, *91*, 054110.

(60) Grimme, S. Semiempirical GGA-type Density Functional Constructed with a Long-Range Dispersion Correction. *J. Comput. Chem.* **2006**, *27*, 1787-1799.

(61) Steinhardt, P. J.; Nelson, D. R.; Ronchetti, M. Bond-Orientational Order in Liquids and Glasses. *Phys. Rev. B* **1983**, *28*, 784.

(62) van Duijneveldt, J. S.; Frenkel, D. Computer Simulation Study of Free Energy Barriers in Crystal Nucleation. *J. Chem. Phys.* **1992**, *96*, 4655-4668.

(63) Lechner, W.; Dellago, C. Accurate Determination of Crystal Structures Based on Averaged Local Bond Order Parameters. *J. Chem. Phys.* **2008**, *129*, 114707-5.

(64) Kelton, K. F.; Weinberg M. C. Calculation of Macroscopic Growth Rates from Nucleation Data. *J. Non-Cryst. Solids* **1994**, *180*, 17-24.

(65) Santala, M. K.; Reed, B. W.; Raoux, S.; Topuria, T.; LaGrange, T.; Campbell, G. H. Irreversible Reactions Studied with Nanosecond transmission Electron Microscopy Movies: Laser Crystallization of Phase Change Materials. *Appl. Phys. Lett.* **2013**, *102*, 174105.

(66) Thomson, C. V.; Spaepen, F. On the Approximation of the Free Energy Change on Crystallization. *Acta Metallurg.* **1979**, *27*, 1855-1859.

(67) Fantini, P.; Brazzelli, S.; Cazzini, E.; Mani, A. Band Gap Widening with Time Induced by Structural Relaxation in Amorphous $Ge_2Sb_2Te_5$ Films. *Appl. Phys. Lett.* **2012**, *100*, 013505.

(68) VandeVondele, J.; Krack, M.; Mohamed, F.; Parrinello, M.; Chassaing, T.; Hutter, J. QUICKSTEP: Fast and Accurate Density Functional Calculations Using a Mixed Gaussian and Plane Waves Approach. *Comput. Phys. Commun.* **2005**, *167*, 103-128; www.cp2k.org.

(69) Engel, E.; Vosko, S. H. Exact Exchange-Only Potentials and the Virial Relation as Microscopic Criteria for Generalized Gradient Approximations. *Phys. Rev. B* **1993**, *47*, 13164-13174.

(70) Caravati, S.; Bernasconi, M.; Kuehne, T. D.; Krack, M.; Parrinello, M. First-Principles Study of Crystalline and Amorphous $Ge_2Sb_2Te_5$ and the Effects of Stoichiometric Defects. *J. Phys.: Condens. Matter* **2009**, *21*, 255501.

(71) Laio, A.; Parrinello, M. Escaping Free-Energy Minima. *Proc. Nat. Acad. Sci.* **2002**, *99*, 12562-12566; Laio, A.; Gervasio, F. L. Metadynamics: a Method to Simulate Rare Events and Reconstruct the Free Energy in Biophysics, Chemistry and Material Science. *Rep. Prog. Phys.* **2008**, *71*, 126601; Barducci, A.; Bonomi, M.; Parrinello, M. Metadynamics. *Wires Comp. Mat. Sci.* **2011**, *1*, 826-843.

(72) Caravati, S.; Bernasconi, M.; Parrinello, M. First Principles Study of the Optical Contrast in Phase Change Materials. *J. Phys.: Condens. Matter* **2010**, *22*, 315801.

(73) Mitrofanov, K. V.; Kolobov, A. V.; Fons, P.; Wang, X.; Tominaga, J.; Tamenori, Y.; Uruga, T.; Ciocchini, N.; Ielmini, D. Ge L-3-edge x-ray Absorption Near-Edge Structure Study of Structural Changes Accompanying Conductivity Drift in the Amorphous Phase of $Ge_2Sb_2Te_5$. *J. Appl. Phys.* **2014**, *115*, 173501.

(74) Raty, J. Y.; Zhang, W.; Luckas, J.; Chen, C.; Mazzarello, R.; Bichara, C.; Wuttig, M. Aging Mechanisms in Amorphous Phase-Change Materials. *Nature Comm.* **2015**, *7*, 7467.

(75) Rütten, M.; Kaes, M.; Albert, A.; Wuttig, M.; Salinga, M. Relation between Bandgap and Resistance Drift in Amorphous Phase Change Materials. *Sci. Rep.* **2015**, *5*, 17362.

(76) Caravati, S.; Bernasconi, M. Influence of the Exchange and Correlation Functional on the Structure of Amorphous $Ge_2Sb_2Te_5$. *Physica Status Solidi B* **2015**, *252*, 260-266.

(77) Caravati, S.; Bernasconi, M.; Parrinello, M. First-Principles Study of Liquid and Amorphous Sb_2Te_3. *Phys. Rev. B*, **2010**, *81*, 014201.

(78) Zipoli, F.; Krebs, D.; Curioni, A. Structural Origin of Resistance Drift in Amorphous GeTe. *Phys. Rev. B* **2016**, *93*, 115201.